minerals

MDPI

Article

Alteration of Feldspathoids Changes pH of Late-Magmatic Fluids: A Case Study from the Lovozero Peralkaline Massif, Russia

Julia A. Mikhailova [1,*], Yakov A. Pakhomovsky [1], Lyudmila M. Lyalina [1] and Ekaterina A. Selivanova [1,2]

[1] Geological Institute, Kola Science Centre, Russian Academy of Sciences, 184209 Apatity, Russia
[2] Nanomaterials Research Centre, Kola Science Centre, Russian Academy of Sciences, 184209 Apatity, Russia
* Correspondence: mikhailova@geoksc.apatity.ru; Tel.: +7-81555-79333

Abstract: The 360-370-Ma-old Lovozero peralkaline massif (NW Russia) is a layered nepheline syenitic–foidolitic pluton. In the rocks of the massif, late-stage (auto)metasomatic alterations of rock-forming minerals are quite intense. We studied the products of the alteration of nepheline and sodalite via microtextural, microprobe, and spectroscopic methods. We found that these minerals are extensively replaced by the association between natrolite + nordstrandite ± böhmite ± paranatrolite in accordance with the following reactions: 3Nph + 4H_2O → Ntr + Nsd + NaOH; 6Nph + 9H_2O → Ntr + Pntr + 2Nsd + 2NaOH; Sdl + 4H_2O → Ntr + Nsd + NaOH + NaCl, where Nph is nepheline, Ntr is natrolite, Nsd is nordstrandite, Pntr is paranatrolite, and Sdl is sodalite. As a result, about one-third of the sodium from nepheline (and sodalite) is set free and passes into the fluid. This leads to an increase in the Na/Cl ratio and, hence, the pH of the fluid. An increase in pH stabilizes hyperagpaitic minerals (e.g., ussingite, villiaumite, thermonatrite, and trona), which can crystallize in close proximity to pseudomorphized nepheline and sodalite. Thus, the alteration of feldspathoids increases the pH of late-magmatic fluids, which in turn can lead to the crystallization of hyperagpaitic minerals.

Keywords: feldspathoids; secondary alteration; Lovozero massif; natrolite

Citation: Mikhailova, J.A.; Pakhomovsky, Y.A.; Lyalina, L.M.; Selivanova, E.A. Alteration of Feldspathoids Changes pH of Late-Magmatic Fluids: A Case Study from the Lovozero Peralkaline Massif, Russia. *Minerals* **2023**, *13*, 39. https://doi.org/10.3390/min13010039

Academic Editors: Jan Marten Huizenga and Pei Ni

Received: 20 September 2022
Revised: 21 December 2022
Accepted: 23 December 2022
Published: 26 December 2022

1. Introduction

Peralkaline igneous rocks (molar (Na + K)/Al ratio > 1) include intrusive and volcanic silica-oversaturated (granitic/rhyolitic), silica-saturated (syenitic/trachytic), and silica-undersaturated (nepheline syenitic–foidolitic/phonolitic–foiditic) rocks [1,2]. In general, peralkaline rocks crystallize from highly evolved mantle-derived melts [3–5] and typically show exceptionally high concentrations of the large-ion lithophile elements (LILE), such as Na, K, and Li, and the high field strength elements (HFSE), such as rare earth elements (REE), Nb, Ta, Ti, Zr, U, and Th, potentially forming ore deposits of these elements [6,7]. Peralkaline rocks are subdivided into miaskitic, agpaitic, transitional agpaitic, and hyperagpaitic varieties, depending on their mineralogy [2]. Rocks should be termed as miaskitic if the major primary magmatic HFSE carriers are zircon/baddeleyite and titanite/perovskite. Index minerals of agpaitic rocks are complex Na-Ca-HFSE minerals, such as minerals of the eudialyte, rinkite, and wöhlerite groups. Transitional agpaitic rocks contain minerals typical of both agpaitic and miaskite rocks, such as titanite and eudialyte-group minerals. Index minerals of hyperagpaitic rocks are ussingite, naujakasite, steenstrupine-(Ce), minerals of the lomonosovite and lovozerite groups, and water-soluble minerals (e.g., villiaumite and natrosilite).

Subsequent to a primary magmatic phase with comparatively low liquidus temperatures of 500 to 400 °C [8], late-stage autometasomatic reactions are described for peralkaline rocks, implying the release of hydrothermal fluids from the magma at temperatures

below 300 °C [9]. Such late-stage reactions result in the modification of previously crystallized minerals and in the stabilization of new phases. Zeolitization is one of the most common late-stage autometasomatic processes in peralkaline rocks, when zeolites, such as minerals of the natrolite group (natrolite, mesolite, gonnardite, and thomsonite) and analcime, replace early formed minerals. In particular, hydrothermally altered phonolitic rocks in the Kaiserstuhl Volcanic Complex, Germany, are of economic interest due to the occurrence of zeolites, dominantly natrolite-group minerals, and analcime [10]. In the Mont Saint–Hilaire peralkaline complex, Canada, Schilling et al. [11] observed analcime and natrolite in syenitic rocks. They determined that these zeolites were formed in a late-magmatic hydrothermal stage, associated with a continuous decrease in silica activity and an increase in water activity due to the consumption of primary igneous nepheline.

One of the world's largest alkaline intrusions is the Lovozero massif located on the Kola Peninsula, Russia. Lovozero is mainly composed of nepheline syenites and foidolites, and the intensity of late-stage autometasomatic processes is extremely high here. We studied the products of alteration of nepheline and sodalite from various lithologies of the Lovozero massif using microtextural, microprobe, and spectroscopic methods. We found that these minerals are extensively replaced by the association between natrolite + nordstrandite ± böhmite ± paranatrolite. In this article, we present the results of our research and discuss possible replacement reactions resulting in changes in the pH of late-magmatic fluids.

2. Geological Background and Short Petrography Description

The Lovozero layered laccolith-type intrusion (Figure 1) is located on the Kola Peninsula (Russia) and covers an area of 650 km^2. It was emplaced 360–370 Ma ago [3,12,13] into Archean granite gneisses covered by Devonian volcaniclastic rocks [14]. The Lovozero massif is composed of three major units [15–17], namely, Layered, Eudialyte, and Poikilitic complexes.

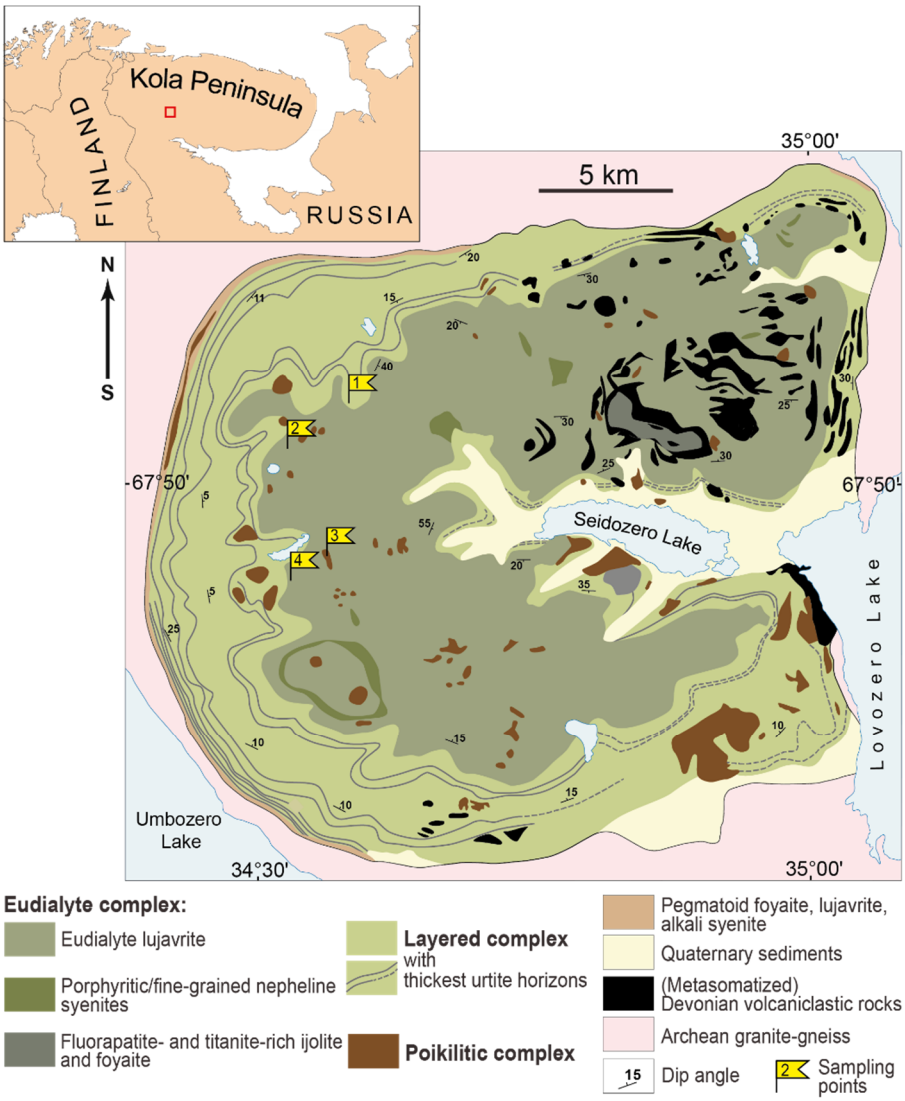

Figure 1. Geological scheme of the Lovozero alkaline massif after [16].

The Layered complex (77% of the massif's volume; about 1.7 km in thickness) consists of numerous sub-horizontal layers or "rhythms". Each rhythm is a sequence of rocks (from top to bottom): lujavrite–foyaite–urtite or lujavrite–foyaite. Lujavrite is trachytoid meso- to melanocratic nepheline syenite; foyaite is massive leucocratic nepheline syenite, and urtite is almost a monomineral nepheline rock (Table 1). The transitions between different rocks within the same rhythm are gradual, and the boundaries between the rhythms are sharp and are often marked by pegmatites.

Table 1. Summary of the petrography of the plutonic rocks of the Lovozero massif.

Complex	Rock	Rock-Forming Minerals (Average Content, mod. %)	Characteristic Accessory Minerals [1]	Texture
Layered	Lujavrite	Microcline-perthite (45), nepheline + secondary natrolite (20), aegirine (25), magnesio-arfvedsonite (5)	EGM [2], lamprophyllite, sodalite, loparite-(Ce), barytolamprophyllite, sphalerite, fluorapatite, lorenzenite	Trachytoid; coarse- to medium-grained
	Foyaite	Microcline-perthite (50), nepheline + secondary natrolite (35), aegirine (7)	Magnesio-arfvedsonite, EGM, sodalite, lamprophyllite, sphalerite, loparite-(Ce), murmanite, lomonosovite	Massif to weakly trachytoid; coarse- to medium-grained

	Urtite	Nepheline + secondary natrolite (70), microcline-perthite (12), sodalite (7), aegirine (6)	Loparite-(Ce), fluorapatite, EGM, magnesio-arfvedsonite, titanite, murmanite, sphalerite	Massif; coarse- to medium-grained
Eudialyte	Eudialyte lujavrite	Microcline-perthite (35), EGM (25), aegirine (20), nepheline + secondary natrolite (15), magnesio-arfvedsonite (5)	Sodalite, loparite-(Ce), lamprophyllite, barytolamprophyllite, sphalerite	Trachytoid; coarse- to medium-grained
	Foyaite	Microcline-perthite (55), nepheline + secondary natrolite (35), aegirine (7)	Magnesio-arfvedsonite, fluorapatite, sodalite, lovozerite-group minerals, EGM, murmanite, lomonosovite	Massif to weakly trachytoid; coarse- to medium-grained
	Porphyritic/ fine-grained nepheline syenites	Fine-grained mass: albite (25), microcline (25), nepheline (20), aegirine (20), magnesio-arfvedsonite (5) Phenocrysts: nepheline (0–20), microcline-perthite (0–35)	EGM, lovozerite-group minerals, sodalite, murmanite, lamprophyllite	Porphyritic/ fine-grained
Poikilitic	Uneven-grained nepheline syenite	Microcline-perthite, nepheline, magnesio-arfvedsonite, aegirine, orthoclase	Titanite, fluorapatite, ilmenite, diopside, EGM	Metasomatic, poikilitic
	Poikilitic foid syenite	Orthoclase, sodalite, vishnevite, nepheline, cancrinite, katophorite, aegirine	Titanite, fluorapatite, ilmenite, diopside, phlogopite, EGM, zircon	Metasomatic, poikilitic

[1] Ranked in order of decreasing importance; [2] eudialyte-group minerals. For rocks of the Poikilitic complex, the average content of minerals is not given since the modal composition varies very significantly.

The Eudialyte complex (18% of massif's volume; thickness varies from 0.1 to 0.8 km) overlies the Layered complex and consists of lujavrite enriched in eudialyte-group minerals, so-called eudialyte lujavrite. Lenses and sheet-like bodies of foyaite, as well as fine-grained/porphyritic nepheline syenites (Table 1), are irregularly located among eudialyte lujavrite.

The Poikilitic complex (5% of massif's volume) consists of leucocratic feldspathoid syenites, in which grains of feldspathoids are poikilitically incorporated into large crystals of alkali feldspar. These rocks form lenses, or irregularly shaped bodies, which are located in both the Layered and Eudialyte complexes. In the Poikilitic complex, the following main groups of rocks are recognized (Table 1): uneven-grained nepheline syenite and poikilitic foid syenite. These rocks are connected by gradual transitions but differ in the content of poikilitic feldspar crystals.

A large number of xenoliths of Devonian volcaniclastic rocks [14,15], both unaltered and intensely metasomatized (fenitized), are found among the rocks of the Layered and Eudialyte complexes. Alkaline lamprophyre dikes of up to 5 m thick are most common in the northwest and south of the Lovozero massif.

3. Materials and Methods

The materials for the study were samples of the most common rocks of the Lovozero massif, namely lujavrite, foyaite, and urtite of the Layered complex, eudialyte lujavrite of the Eudialyte complex, as well as poikilitic foid syenite from the Poikilitic complex. A total of 23 samples were collected (Table 2). The sampling points are shown in Figure 1, and the sample study sequence is shown in Figure 2.

Table 2. List of studied samples.

Sampling Point	Sample	Rock	Complex
1	LV-319A	lujavrite	Layered
1	LV-335/4	foyaite	Layered
1	LV-319G	urtite	Layered
1	LV-335/6	urtite	Layered
1	LV-335/2	urtite	Layered
1	LV-315/1	urtite	Layered
1	LV-335/3	urtite	Layered
1	LV-306	urtite	Layered
1	LV-303/2	urtite	Layered
1	LV-319/3	urtite	Layered
1	LV-319/2	urtite	Layered
1	LV-420	foyaite	Eudialyte
2	LV-366A-2	eudialyte lujavrite	Eudialyte
2	LV-335E-1	eudialyte lujavrite	Eudialyte
2	LV-350/1	eudialyte lujavrite	Eudialyte
2	LV-354/2	poikilitic foid syenite	Poikilitic
3	LV-356/3	poikilitic foid syenite	Poikilitic
3	LV-382/4	poikilitic foid syenite	Poikilitic
3	LV-384/1	eudialyte lujavrite	Eudialyte
3	LV-377/2	eudialyte lujavrite	Eudialyte
4	LV-363/17	urtite	Layered
4	LV-363/6	foyaite	Eudialyte
4	LV-363/18	foyaite	Eudialyte

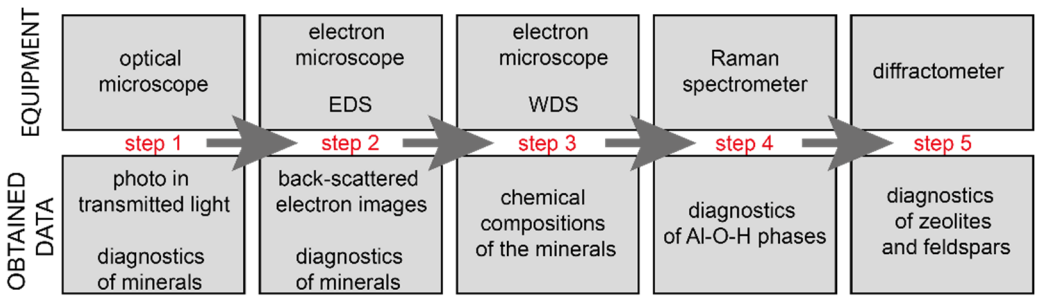

Figure 2. Samples study sequence. Zeolites were identified both by chemical composition (steps 2 and 3) and by X-ray diffraction analysis (step 5). Al-O-H phases (nordstrandite and böhmite) were identified both by chemical composition (steps 2 and 3) and by Raman spectra (step 4). The figure does not show step 6, namely, the determination of the chemical composition of the rock.

Microprobe analyses of minerals were performed at the Geological Institute, Kola Science Center of the Russian Academy of Sciences (GI KSC RAS, Apatity, Russia), using the Cameca MS-46 electron microprobe (Cameca, Gennevilliers, France) operating in the WDS mode at 22 kV with a beam diameter of 10 μm, a beam current of 20–40 nA, and counting times of 10 s (for a peak) and 10 s (for background before and after the peak), with 5–10 counts for every element in each point. The following standards were used: lorenzenite (Na), pyrope (Al), wollastonite (Si), wadeite (K), hematite (Fe), atacamite (Cl), and $Fe_{10}S_{11}$ (S). The analytical precision (reproducibility) of mineral analyses was 0.2–0.05 wt% (two standard deviations) for the major element and approximately 0.01 wt% for impurities. The systematic errors were within the random errors. Backscattered electron (BSE) images were obtained using a scanning electron microscope LEO-1450 (Carl Zeiss Microscopy, Oberkochen, Germany) with the energy-dispersive system (EDS) Aztec Ultimmax 100 (Oxford Instruments, Oxford, UK).

The whole-rock major element chemistry was determined through a wet chemical analysis at the GI KSC RAS. The accuracy limits of the wet chemical analysis for SiO_2, TiO_2, ZrO_2, Fe_2O_3, Al_2O_3, CaO, SrO, MgO, MnO, Na_2O, K_2O, P_2O_5, S_{tot}, Cl, and H_2O are 0.01 wt.%, and for FeO and CO_2, they are 0.1 wt.%. The accuracy limit for F is 0.001 wt.%.

The X-ray diffraction (XRD) measurements were performed at the Kola Science Center using a MiniFlex-600 powder diffractometer (Rigaku Corporation, Tokyo, Japan). The X-ray source was CuKα radiation. The tube current and the tube voltage were set at 15 mA and 40 kV, respectively. A one-dimensional detector (D/teX Ultra2, Rigaku Corporation, Tokyo, Japan) was used with a K_β filter. XRD data were identified using the RRUFF Project database [18]. The Raman spectra collected from uncoated individual grains were recorded with a Horiba Jobin-Yvon LabRAM HR800 spectrometer equipped with an Olympus BX-41 microscope in backscattering geometry (Saint-Petersburg State University). Raman spectra were excited using a solid-state laser (532 nm) with an actual power of 2 mW under the 50× objective (NA 0.75). The spectra were obtained in the range of 70–4000 cm^{-1} at a resolution of 2 cm^{-1} at room temperature. To improve the signal-to-noise ratio, the number of acquisitions was set to 15. The spectra were processed using the algorithms implemented in the Labspec and OriginPro 8.1 software packages (Originlab Corporation, Northampton, MA, USA).

The ImageJ open-source image processing program (https://imagej.nih.gov/ij/) was used to create digital images from the BSE images and to determine the ratio of the areas occupied by each of the nepheline alteration products. The program *STATISTICA* 12 (StatSoft) was used to construct the isocon diagram. Mineral abbreviations (Table 3) are given in accordance with IMA (International Mineralogical Association)-approved mineral symbols [19], with the exception of the eudialyte-group minerals (EGM).

Table 3. Abbreviations, names, and formulas of minerals mentioned in this article.

Abbreviation [19]	Mineral	Formula [1]
Ab	albite	$Na(AlSi_3O_8)$
Aeg	aegirine	$NaFe^{3+}Si_2O_6$
Anl	analcime	$Na(AlSi_2O_6)\cdot H_2O$
Bhm	böhmite	AlO(OH)
EGM	eudialyte-group mineral	[20]
Fap	fluorapatite	$Ca_5(PO_4)_3F$
Gon	gonnardite	$(Na,Ca)_2(Si,Al)_5O_{10}\cdot 3H_2O$
Gth	goethite	FeO(OH)
Lmp	lamprophyllite	$(SrNa)Ti_2Na_3Ti(Si_2O_7)_2O_2(OH)_2$
Lop-Ce	loparite-(Ce)	$(Na,Ce,Sr)(Ce,Th)(Ti,Nb)_2O_6$
Lvz	lovozerite	$Na_3CaZrSi_6O_{15}(OH)_3$
Marf	magnesio-arfvedsonite	$NaNa_2(Mg_4Fe^{3+})Si_8O_{22}(OH)_2$
Mcc	microcline	$K(AlSi_3O_8)$
Mes	mesolite	$Na_2Ca_2(Si_9Al_6)O_{30}\cdot 8H_2O$
Mmn	murmanite	$Na_2Ti_2Na_2Ti_2(Si_2O_7)_2O_4(H_2O)_4$
Nj	naujakasite	$Na_6Fe^{2+}Al_4Si_8O_{26}$
Nph	nepheline	$Na_3K(Al_4Si_4O_{16})$
Ns	natrosilite	$Na_2Si_2O_5$
Nsd	nordstrandite	$Al(OH)_3$
Ntr	natrolite	$Na_2(Si_3Al_2)O_{10}\cdot 2H_2O$
Pntr	paranatrolite	$Na_2(Si_3Al_2)O_{10}\cdot 3H_2O$
Py	pyrite	FeS_2
Rha-La	rhabdophane-(La)	$La(PO_4)\cdot H_2O$
Sdl	sodalite	$Na_4(Si_3Al_3)O_{12}Cl$

Ssp-Ce	steenstrupine-(Ce)	$Na_{14}Ce_6Mn^{2+}_2Fe^{3+}_2Zr(PO_4)_7Si_{12}O_{36}(OH)_2 \cdot 3H_2O$
Thm-Ca	thomsonite-Ca	$NaCa_2(Al_5Si_5)O_{20} \cdot 6H_2O$
Tn	trona	$Na_3(HCO_3)(CO_3) \cdot 2H_2O$
Tnat	thermonatrite	$Na_2(CO_3) \cdot H_2O$
Ttp	tugtupite	$Na_4BeAlSi_4O_{12}Cl$
Usg	ussingite	$Na_2AlSi_3O_8(OH)$
Vll	villiaumite	NaF

[1] Formulas are given in accordance with IMA (International Mineralogical Association) list of minerals, with the exception of eudialyte-group minerals (EGM).

4. Results

4.1. Petrography

4.1.1. Alteration of Nepheline and Sodalite in the Layered Complex

Eu- to subhedral nepheline (up to 1 cm across) is a rock-forming mineral in all rock types of the Layered complex (Table 1) and often contains numerous inclusions of small needle-like aegirine crystals. Sodalite is a characteristic accessory mineral of the lujavrite and foyaite of the Layered complex, while in urtite, the content of sodalite reaches 15 mod. %. As a rule, sodalite forms rounded grains up to 3 mm across.

In lujavrite of the Layered complex (Figure 3a), both sodalite and nepheline are intensively replaced by an aggregate of natrolite and nordstrandite (Figure 3b–d) up to the formation of complete pseudomorphs. Nordstrandite is represented by irregularly shaped grains of up to 40 μm across, evenly distributed in the aggregate of fine-grained natrolite (Figure 3d). Small (up to 8 μm across) pyrite and goethite grains are found in association with natrolite and nordstrandite (Figure 3c,d). Pseudomorphized nepheline is easy to recognize microscopically as it is almost opaque and has a light brown color (Figure 3a). Along with natrolite, which replaces nepheline, lujavrite contains primary natrolite [21], forming anhedral transparent grains among rock-forming minerals.

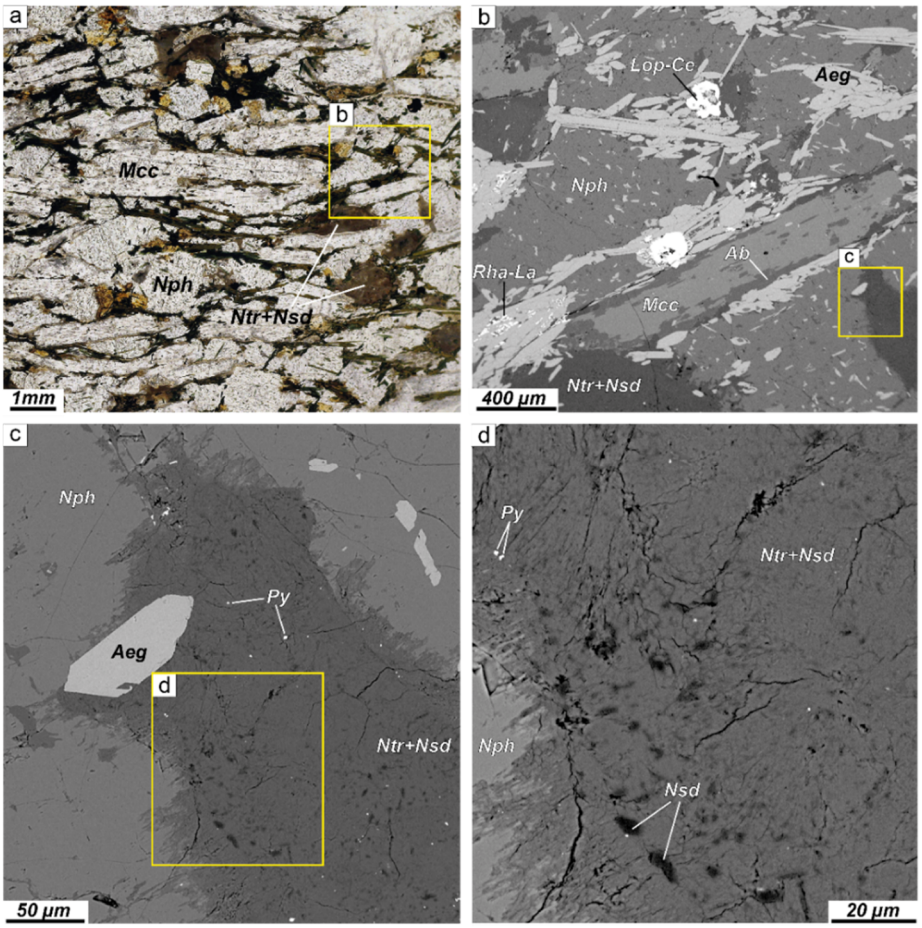

Figure 3. Replacement of nepheline with natrolite + nordstrandite aggregate in lujavrite of the Layered complex. (**a**) Cloudy, opaque areas occupied by the secondary natrolite + nordstrandite aggregates; photo of a thin section under transmitted light; (**b**) intensive replacement of nepheline with an aggregate of natrolite and nordstrandite along grain boundaries; BSE image; (**c**) and (**d**) detailed BSE images of nepheline alteration products. Sample LV-319A.

In the foyaite of the Layered complex, nepheline and sodalite are extensively replaced by the natrolite + nordstrandite + böhmite assemblage (Figure 4a,b). It is important to note that albite in foyaite is intensely replaced by natrolite. Figures 4c,d shows the boundary between natrolite replacing albite and the natrolite + nordstrandite + böhmite association replacing nepheline.

Nordstrandite and böhmite form small irregular grains of up to 40 μm across. Both the Al-O-H-phases (nordstrandite and böhmite) occur together and are evenly distributed in the mass of natrolite (Figure 4b–e). Nordstrandite and böhmite show distinct different Raman spectra (Figure 4e–g). In association with natrolite, nordstrandite, and böhmite, there are also small grains of goethite, pyrite, and rarely hematite, manganese oxides, and hydroxides. In foyaite, as in lujavrite, in addition to secondary natrolite, there is also primary transparent natrolite, which fills the spaces between grains of rock-forming minerals.

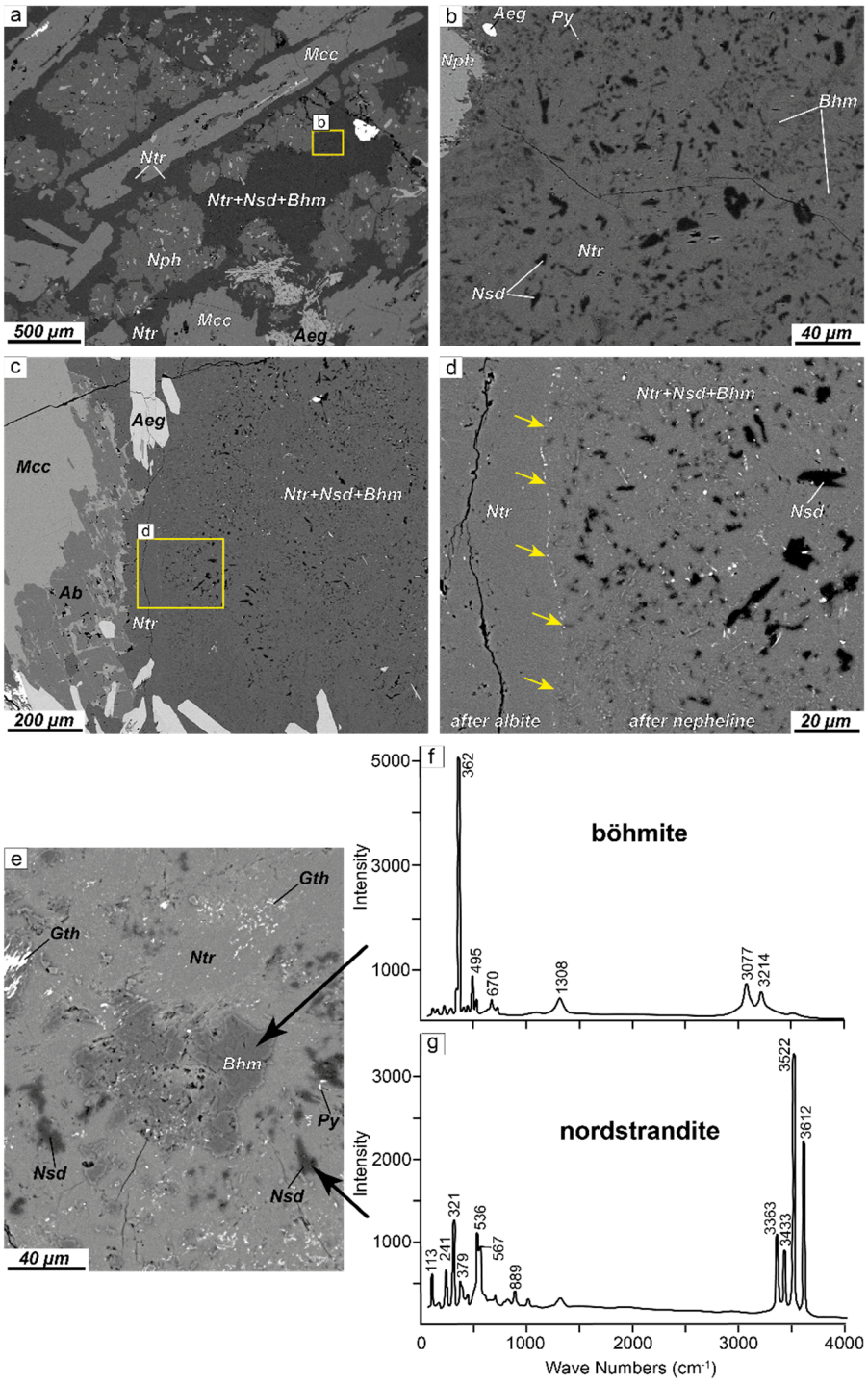

Figure 4. Secondary alteration of nepheline and albite in foyaite from the Layered complex. (**a**) Replacement of nepheline by an aggregate of natrolite, nordstrandite, and böhmite; BSE image; (**b**) detailed BSE image of Figure 4a; (**c**) albite is replaced by natrolite (left), while nepheline is replaced by the natrolite + nordstrandite + böehmite association (right); BSE image; (**d**) detailed BSE image of Figure 4c; yellow arrows mark the boundary between natrolite replacing albite and the natrolite + nordstrandite + böehmite association replacing nepheline; (**e**) association of secondary minerals replacing nepheline; BSE image; (**f**) and (**g**) Raman spectra of böhmite and nordstrandite, respectively. Sample LV-335/4.

In the urtite of the Layered complex, nepheline and sodalite are ubiquitously replaced by an aggregate of natrolite + nordstrandite ± paranatrolite (Figure 5a,b) or natrolite + nordstrandite + böhmite (Figure 5c,d), up to the formation of complete pseudomorphs. Nordstrandite and böhmite form small (up to 50 μm) irregularly shaped grains (Figure 5b,d), evenly distributed in the mass of natrolite (and paranatrolite). Goethite and pyrite are constantly present in association with the natrolite, paranatrolite, and Al-O-H phases. In addition to secondary natrolite, urtite contains primary transparent homogeneous natrolite, which fills the intergranular space of nepheline grains, as well as the space between pseudomorphs after nepheline (Figure 5e,f).

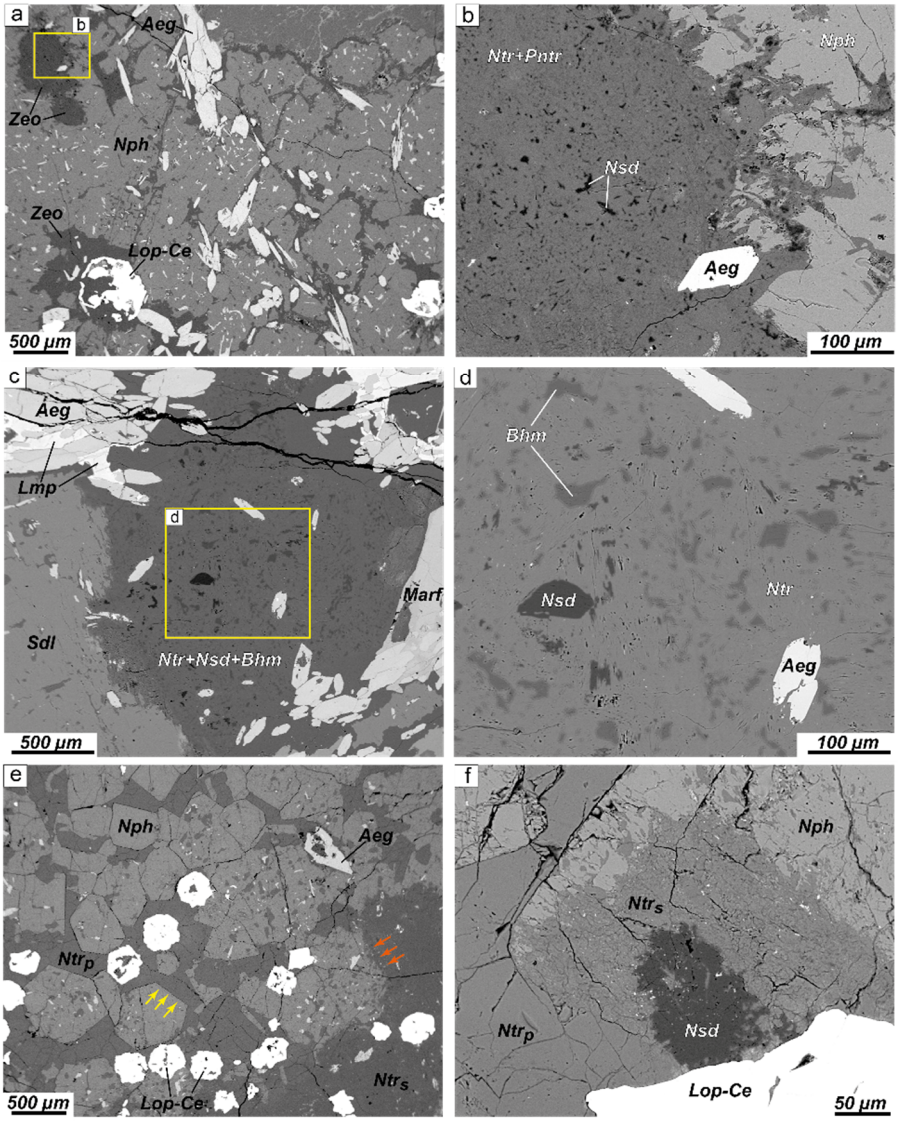

Figure 5. Secondary alteration of nepheline and sodalite in urtite from the Layered complex. (**a**) Alteration of nepheline by an aggregate of natrolite + paranatrolite + nordstrandite (Zeo); BSE-image; (**b**) detailed BSE-image of the Figure 5a; (**c**) alteration of sodalite by an aggregate of natrolite + nordstrandite + böhmite; BSE image; (**d**) detailed BSE image of Figure 5c; (**e**) primary natrolite filling the intergranular space of nepheline grains (left side of the figure) and secondary aggregates natrolite + paranatrolite + nordstrandite replacing nepheline (right side of the figure). The yellow arrows indicate the primary natrolite/nepheline boundary (no alteration), the orange arrows indicate the secondary natrolite/nepheline boundary; BSE image; (**f**) relationship between primary and secondary natrolite; BSE image. Ntr_P—primary natrolite; Ntr_S—secondary natrolite; Zeo—natrolite + paranatrolite + nordstrandite. Samples LV-319G (**a,b**), LV-335/6 (**c,d**), and LV-363/17 (**e,f**).

4.1.2. Alteration of Nepheline and Sodalite in the Eudialyte Complex

In the eudialyte lujavrite and foyaite of the Eudialyte complex, nepheline and sodalite are extensively replaced by natrolite + nordstrandite + böhmite and/or the natrolite + paranatrolite + nordstrandite + böhmite associations (Figure 6a–d). Aggregates containing paranatrolite are usually looser and porous. Nordstrandite and böhmite form small, irregular grains that are evenly distributed among natrolite/paranatrolite. Large nordstrandite grains (up to 200 μm across) are encountered, around which small grains of nordstrandite are absent (Figure 6b). Together with the Al-O-H phases, zeolite aggregates contain small grains of pyrite, pyrrhotite, and goethite (Figure 6b,d).

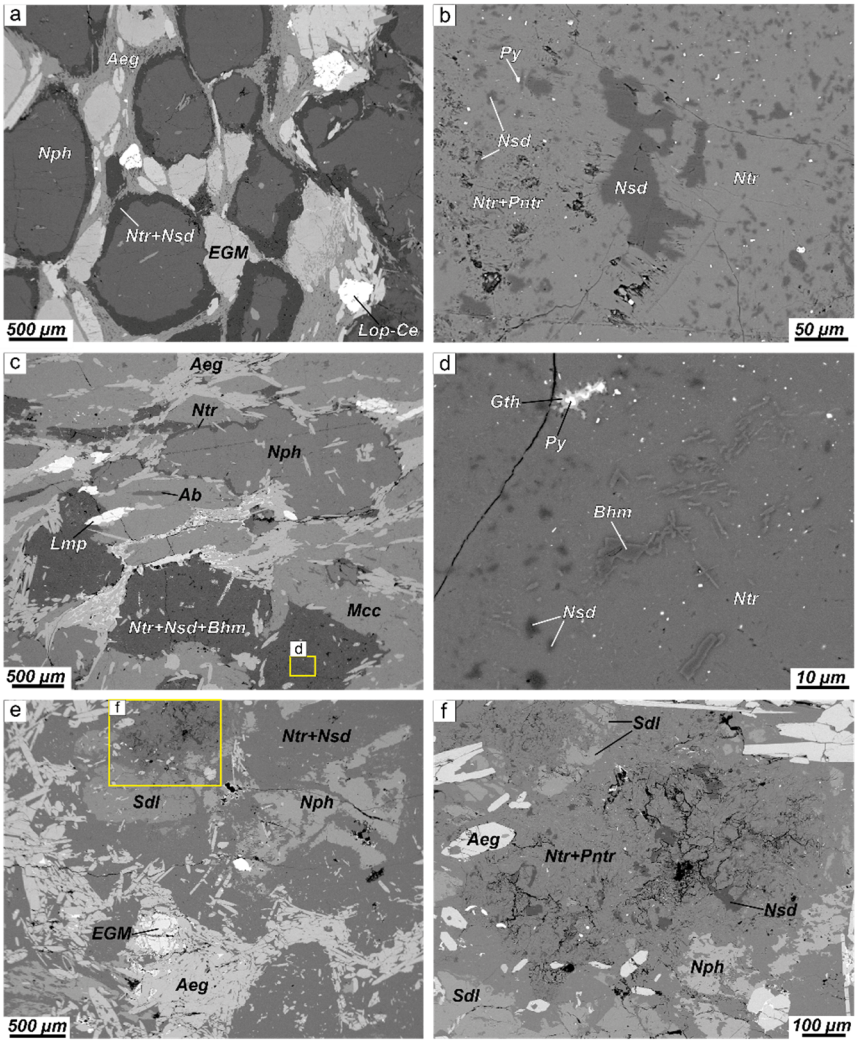

Figure 6. Secondary alteration of nepheline and sodalite in rocks from the Eudialyte and Poikilitic complexes. (**a**) Replacement of nepheline with natrolite and nordstrandite in eudialyte lujavrite from the Eudialyte complex; (**b**) nepheline alteration products in eudialyte lujavrite from the Eudialyte complex; sample LV-350/1; (**c**) pseudomorphs of natrolite + nordstrandite + böhmite after nepheline in lujavrite from the Eudialyte complex; (**d**) nepheline alteration products in lujavrite from the Eudialyte complex; sample LV-377/2; (**e**) replacement of nepheline and sodalite by an assemblage of secondary minerals including natrolite, paranatrolite, and nordstrandite in poikilitic sodalite syenite from the Poikilitic complex; (**f**) nepheline alteration products in poikilitic sodalite syenite from the Poikilitic complex; sample LV-356/3. BSE-images.

4.1.3. Alteration of Nepheline and Sodalite in the Poikilitic Complex

In the rocks of the Poikilitic complex, the replacement of feldspathoids by an association of secondary minerals is as intense as in the urtite of the Layered Complex. Often, feldspathoids are preserved only as small relics in the mass of natrolite, paranatrolite, nordstrandite, and böhmite (Figure 6e). Natrolite and paranatrolite are the predominant zeolites, but gonnardite and thomsonite are also present in the mass of secondary zeolites. Areas composed of the mineral association natrolite + nordstrandite + böhmite are denser and more uniform, while areas containing paranatrolite and other zeolites are loose and porous (Figure 6f). Together with the Al-O-H phases, zeolite aggregates contain small grains of pyrite, pyrrhotite, and goethite, as well as manganese hydro(oxides).

4.2. Mineral Chemistry

Representative chemical analyses of unaltered nepheline and sodalite are presented in Tables 4 and 5. Nepheline usually contains an admixture of ferric iron (up to 0.12 *apfu*). In this mineral, there is a constant lack of potassium (minimum content 0.66 *apfu*), compensated with an excess amount of silicon (up to 4.35 *apfu*). Sodalite is characterized by an admixture of sulfur (up to 0.27 *apfu*) and ferric iron (up to 0.05 *apfu*).

Table 4. Representative chemical analyses of nepheline from Lovozero rocks (microprobe, wt. %).

Complex	**Layered**				**Eudialyte**	**Poikilitic**
Rock	**Lujavrite**	**Foyaite**	**Urtite**	**Urtite**	**Eudialyte Lujavrite**	**Poikilitic Sodalite Syenite**
Sample	**LV-319A**	**LV-335/4**	**LV-335/6**	**LV-319G**	**LV-350/1**	**LV-356/3**
SiO_2	42.88	41.42	44.95	41.57	44.80	45.34
Al_2O_3	31.99	33.53	30.79	33.28	31.11	30.11
Fe_2O_3	1.11	0.05	1.65	0.08	1.29	1.70
Na_2O	15.69	15.48	16.27	16.11	16.13	15.88
K_2O	6.63	6.96	5.32	6.97	5.69	5.64
Sum	**98.30**	**97.44**	**98.98**	**98.01**	**99.02**	**98.67**
Formula based on 16 oxygens, *apfu*						
Si	4.21	4.10	4.35	4.10	4.34	4.40
Al	3.70	3.91	3.51	3.87	3.55	3.45
Fe^{3+}	0.08	–	0.12	0.01	0.09	0.12
Na	2.99	2.97	3.05	3.08	3.03	2.99
K	0.83	0.88	0.66	0.88	0.70	0.70
Sum	**11.81**	**11.87**	**11.69**	**11.94**	**11.71**	**11.66**

apfu—atoms per formula unit.

Table 5. Representative chemical analyses of sodalite from Lovozero rocks (microprobe, wt. %).

Complex	**Layered**		**Eudialyte**	**Poikilitic**	
Rock	**Urtite**	**Urtite**	**Eudialyte Lujavrite**	**Poikilitic Sodalite Syenite**	
Sample	**LV-335/6**	**LV-319G**	**LV-350/2**	**LV-356/3**	**LV-356/3**
SiO_2	36.66	37.06	37.06	37.27	37.34
Al_2O_3	31.66	31.12	31.22	30.03	29.87
Fe_2O_3	0.05	0.07	0.15	0.86	0.36
Na_2O	26.24	23.92	25.36	25.96	25.14
Cl	6.17	5.34	4.55	6.25	5.56
S	1.04	0.93	1.78	0.43	0.90
–O=Cl	1.39	1.21	1.41	1.03	1.26

–O=S	0.52	0.47	0.21	0.89	0.45
Sum	**99.90**	**96.77**	**99.18**	**98.20**	**97.47**
	Formula based on Si + Al + Fe^{3+} = 6, *apfu*				
Si	2.97	3.01	3.01	3.05	3.08
Al	3.03	2.98	2.98	2.90	2.90
Fe^{3+}	–	–	0.01	0.05	0.02
Na	4.12	3.77	3.99	4.12	4.02
Cl	0.85	0.74	0.63	0.87	0.78
S	0.16	0.14	0.27	0.07	0.14

apfu—atoms per formula unit.

Representative chemical analyses of natrolite and paranatrolite are shown in Table 6. In each sample studied, zeolites were additionally diagnosed using X-ray diffraction (XRD). Natrolite and paranatrolite differ slightly in chemical composition but can be accurately diagnosed using XRD data. For natrolite, the strongest lines of the powder X-ray diffraction pattern [d, Å (I, %)] are 2.85 (100), 5.89 (85), 2.87 (80), 4.35 (70), 6.55 (60), 3.16 (50), and 3.19 (45). For paranatrolite, the strongest lines of the powder X-ray diffraction pattern [d, Å (I, %)] are 2.94 (100), 5.92 (60), 4.44 (40), 4.78 (30), 6.76 (20), 3.26 (15), and 3.12 (15) [18,22]. Paranatrolite is characterized by an increased aluminum content relative to the ideal Al_2Si_3 ratio. According to Seryotkin and colleagues [23], this is due to the presence of additional positions occupied by potassium.

According to the results of microprobe analyses, the chemical composition of nordstrandite (61.75 wt. % Al_2O_3, sample LV-350/1, Figure 6b) corresponds to the formula $Al(OH)_3$, and the chemical composition of böhmite (83.65 wt. % Al_2O_3, sample LV-335/4, Figure 4e) corresponds to the formula AlO(OH). Nordstrandite and böhmite were additionally diagnosed via Raman spectra (Figure 4f,g).

Table 6. Representative chemical analyses of natrolite and paranatrolite from Lovozero rocks (microprobe, wt. %).

Complex	**Layered**	**Layered**	**Eudialyte**	**Poikilitic**	
Rock	**Foyaite**	**Lujavrite**	**Eudialyte Lujavrite**	**Poikilitic Sodalite Syenite**	
Sample	**LV-335/4**	**LV-319A**	**LV-350/1**	**LV-356/3**	**LV-356/3**
Mineral	**Ntr**	**Ntr**	**Pntr**	**Pntr**	**Pntr**
SiO_2	47.15	47.73	42.92	41.80	41.57
Al_2O_3	27.20	26.58	28.48	31.23	27.90
Na_2O	14.37	14.51	15.17	11.91	13.39
K_2O	bdl	bdl	1.99	3.00	1.98
Sum	**88.72**	**88.82**	**88.56**	**87.94**	**84.84**
	Formula based on Si + Al = 5, *apfu*				
Si	2.98	3.02	2.81	2.66	2.79
Al	2.02	1.98	2.19	2.34	2.21
Na	1.76	1.78	1.92	1.47	1.74
K	–	–	0.17	0.24	0.17
H_2O [1]	2.37	2.36	2.51	2.57	3.39

[1] The difference between 100% and the sum of the analysis was attributed to the water content; bdl—below detection limit; *apfu*—atoms per formula unit.

4.3. The Ratio of the Volumes of Nepheline Substitution Products

As mentioned above, the main products of nepheline alteration are zeolites (mainly natrolite) and Al-O-H phases (nordstrandite ± böhmite). The contents of pyrite, goethite,

and manganese (hydro)oxides are negligible. Zeolites and Al-O-H phases are clearly distinguished in the BSE images (Figure 7a) so that the total area occupied by zeolites and the total area occupied by Al-O-H phases can be measured. For this, the BSE image was binarized, and then, using the program ImageJ (see Materials and Methods), the areas occupied by each of the secondary minerals were calculated. For example, Figure 7a shows a BSE image of nepheline substitution products, and Figure 7b shows a binary pattern of this image. The area occupied by white pixels (Al-O-H phases) is 17.3%, and the area of black pixels (natrolite) is 82.7%.

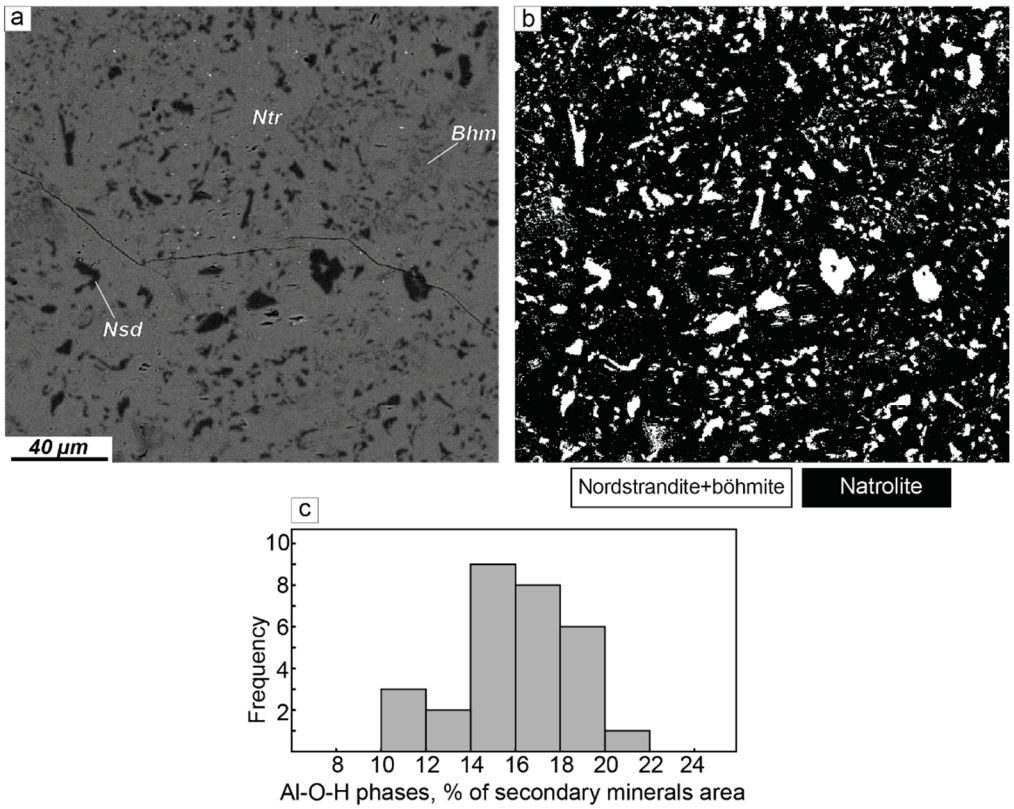

Figure 7. Measurement of areas occupied by nepheline alteration products. (**a**) BSE image of nepheline alteration products (sample LV-335/4); (**b**) binary pattern of Figure 7a, in which black indicates zeolites (82.7% of secondary minerals area), and white indicates nordstrandite + böhmite (17.3% of secondary minerals area); (**c**) bar diagram showing the frequency of samples with different areas occupied by Al-O-H phases.

We analyzed 30 BSE images of nepheline alteration products (Table 7) and found that the ratio of areas occupied by Al-O-H phases and zeolites is quite constant. The area occupied by Al-O-H phases is 11.0–21.1% (median 16.0%) of the total area of alteration products (Figure 7c). Accordingly, the area occupied by zeolites is 78.9–89.2%. Since the grains of nordstrandite and böhmite are isometric in shape, and the zeolites are fine-grained, it can be assumed that the area ratio corresponds to the volume ratio.

Unfortunately, it is not possible to measure the area ratios of sodalite alteration products using the same method since pseudomorphized sodalite is very porous and contains numerous cracks.

Table 7. Results of measurements of areas occupied by nepheline alteration products.

Sample	Rock	Complex	Number of Analyzed BSE-Images	Al-O-H Phases, % of Secondary Minerals Area (Min–Max)	Zeolites, % of Secondary Minerals Area (Min–Max)
LV-319A	lujavrite	Layered	4	10.8–17.5	82.5–89.2
LV-335/4	foyaite	Layered	3	16.8–19.2	80.8–83.2
LV-319G	urtite	Layered	3	15.0–18.2	81.8–85
LV-335/2	urtite	Layered	4	14.9–18.5	81.5–85.1
LV-350/1	eudialyte lujavrite	Eudialyte	3	11.0–15.4	84.6–89
LV-377/2	eudialyte lujavrite	Eudialyte	5	16.2–21.1	78.9–83.8
LV-363/18	foyaite	Eudialyte	2	15.8–16.1	83.9–84.2
LV-363/6	foyaite	Eudialyte	3	14.5–18.2	81.8–85.5
LV-356/3	poikilitic foid syenite	Poikilitic	1	17.6	82.4
LV-382/4	poikilitic foid syenite	Poikilitic	2	16.4–16.7	83.3–83.6

4.4. Changes in the Chemical Compositions of Rocks during the Secondary Alteration of Feldspathoids

To evaluate changes in the chemical composition of rocks at the intensive secondary alteration of feldspathoids, we compared the compositions of fresh urtite and urtite, in which nepheline is replaced by an aggregate of natrolite, paranatrolite, and Al-O-H phases. The chemical analyses of such rocks are shown in Table 8.

Table 8. Chemical compositions of fresh and altered urtite from Layered complex (wt. %).

	Fresh Urtite				Altered Urtite				
Sample	LV-303/2	LV-319/3	LV-319/2	Average of Three Analyses	LV-335/2	LV-335/3	LV-315/1	LV-306	Average of Four Analyses
SiO_2	45.18	45.15	45.03	45.12	47.07	50.12	43.71	43.56	46.12
TiO_2	0.46	0.27	2.03	0.92	0.48	0.39	1.24	0.52	0.66
ZrO_2	0.07	0.04	0.13	0.08	0.06	0.36	0.07	0.08	0.14
Al_2O_3	25.03	28.26	24.61	25.97	23.60	22.87	27.34	24.57	24.60
Fe_2O_3	3.44	1.45	3.87	2.92	2.97	1.84	2.37	2.48	2.42
FeO	1.71	1.10	1.53	1.45	0.65	0.78	0.62	1.41	0.87
MnO	0.12	0.09	0.14	0.12	0.11	0.19	0.12	0.18	0.15
MgO	0.22	0.09	0.37	0.23	0.14	0.13	0.19	0.20	0.17
CaO	1.67	0.10	0.42	0.73	0.27	0.37	0.16	2.48	0.82
SrO	0.44	0.40	0.14	0.33	0.02	0.05	0.12	0.56	0.19
Na_2O	14.82	16.56	14.37	15.25	14.37	12.89	15.63	14.89	14.45
K_2O	3.32	3.56	3.92	3.60	3.07	4.32	3.47	3.17	3.51
P_2O_5	1.35	0.04	0.06	0.48	0.04	0.09	0.04	1.72	0.47
H_2O	0.19	0.31	0.28	0.26	0.35	0.32	0.49	0.49	0.41
CO_2	bdl	bdl	bdl	-	bdl	bdl	bdl	bdl	-
F	0.06	0.02	0.01	0.03	0.01	0.01	0.03	0.08	0.03
Cl	0.10	0.03	0.02	0.05	0.06	0.04	0.11	0.07	0.07
S_{tot}	0.08	0.03	0.05	0.05	0.10	0.01	0.07	0.12	0.08
Loi	1.25	2.57	2.23	2.02	6.96	5.56	3.97	2.92	4.85
Sum	**99.51**	**100.06**	**99.21**		**100.33**	**100.34**	**99.85**	**99.50**	

bdl—below detection limit; Loi—loss on ignition.

To determine which elements were added to or lost from the rock during the alteration of urtite, we used the method of Grant [24,25]. According to this method, the equation for composition–volume relations in metasomatic alteration was written as

$C_i^A = M^O/M^A(C_i^O + \Delta C_i)$,
where C_i is the concentration of component "i";
"O" and "A" refer to the original and altered rocks, respectively;
M^O is the equivalent mass before alteration;
M^A is the equivalent mass after alteration;
ΔC_i is the change in the concentration of component "i".

For each component, there is an equation of this form in which M^O/M^A is constant. If one can identify immobile components, for which $\Delta C_i = 0$, M^O/M^A can be obtained by solving the set of simultaneous equations of the form $C_i^A = (M^O/M^A)C_i^O$. This may be performed graphically by plotting the analytical data against, in which case the immobile components define a straight line through the origin. This is the isocon, whose equation is $C^A = (M^O/M^A)C^O$. The slope of the isocon yields the overall change in mass relative to M^O.

The slope of the isocon can be determined from: (1) the a priori assumption that certain components were immobile; (2) the assumption of constant mass during alteration; (3) the assumption of constant volume during alteration; (4) the clustering of C_i^A/C_i^O data; and (5) the best fit of the data forming a linear array through the origin on an isocon diagram (the graphical method).

Figure 8a is an isocon diagram comparing the chemical composition of fresh urtite (an average of three analyses, Table 8) and altered urtite (an average of four analyses, Table 8). The slope of the isocon was determined from the best fit of data forming a linear array through the origin (the graphical method) [25]. The slope of the isocon is 1.003 (Figure 8a). A slope of 1 (~1.003) indicates that there has been no mass change, whereas higher or lower slopes imply a gain or loss of mass, respectively (or a loss or gain of volume, respectively).

Conclusions that can be drawn from this isocon diagram are that H_2O, Cl, F, S, MnO, ZrO_2, and CaO were added to the rock during alteration, while MgO, SrO, TiO_2, FeO, and Fe_2O_3 were removed. The contents of SiO_2, Al_2O_3, Na_2O, and K_2O remained almost unchanged.

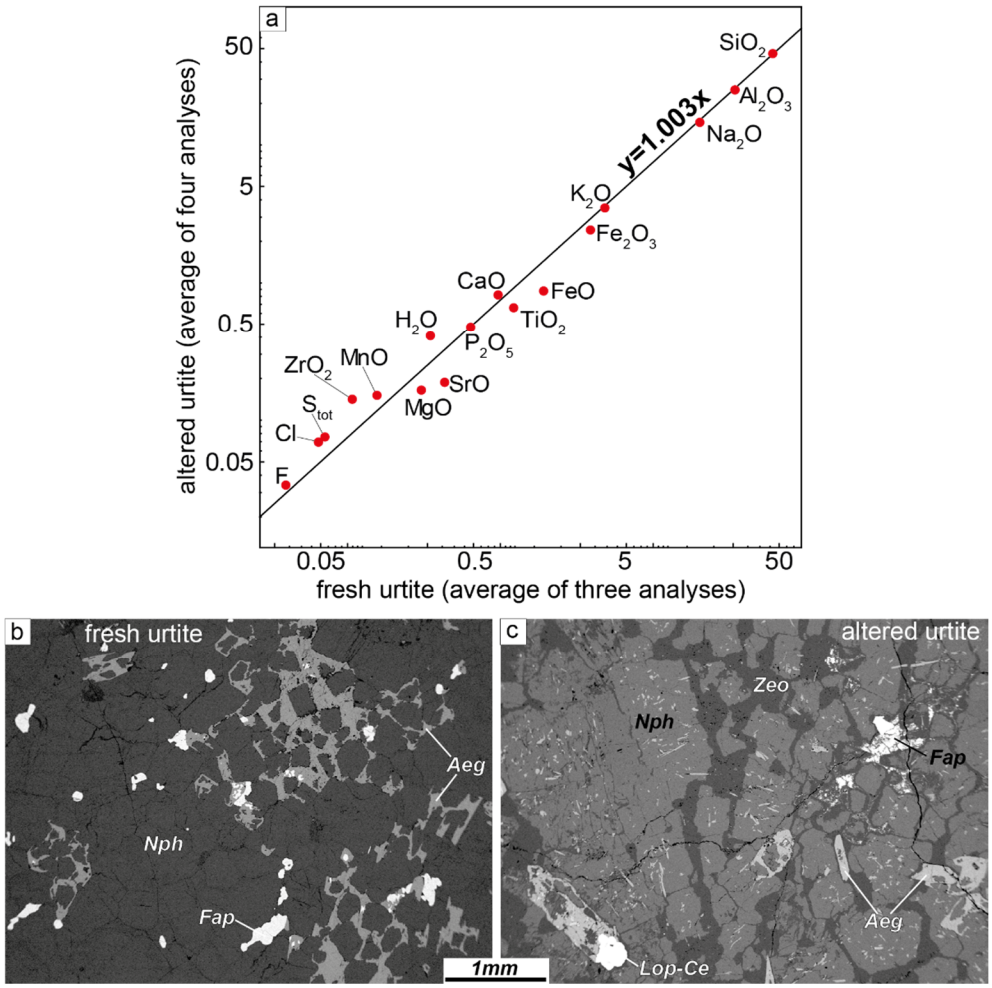

Figure 8. Chemistry of the urtite alteration. (**a**) Isocon diagram comparing the chemistry (in wt. %) of fresh (average of three analyses, Table 8) and altered (average of four analyses, Table 8) urtite from the Layered complex; (**b**) example of fresh urtite (BSE image of sample LV-319/3); secondary alterations of nepheline are not observed; (**c**) example of altered urtite (BSE image of sample LV-335/3); approximately 23% of nepheline is replaced by the natrolite + paranatrolite + nordstrandite aggregate (Zeo).

5. Discussion

Late-stage (auto)metasomatism is typically quite intense and diverse in peralkaline rocks. In this process, the primary magmatic minerals react with aqueous fluids that separate from the same body of magma at a late stage during cooling. In silica-undersaturated (nepheline syenitic–foidolitic) rocks, secondary alterations of feldspathoids are the most intense, leading to the formation of large volumes of secondary zeolites. It is generally accepted that the breakdown of feldspathoid minerals releases the components necessary for zeolite formation according to the following reactions [10,11,26]:

$$2NaAlSiO_4\ (Nph) + SiO_2 + 2H_2O \Rightarrow Na_2Al_2Si_3O_{10}{\cdot}2H_2O\ (Ntr) \quad (1)$$

$$Na_8Al_6Si_6O_{24}Cl_2\ (Sdl) + 3SiO_2 + 6H_2O \Rightarrow 3Na_2Al_2Si_3O_{10}{\cdot}2H_2O\ (Ntr) + 2NaCl \quad (2)$$

$$NaAlSiO_4\ (Nph) + SiO_2 + H_2O \Rightarrow NaAlSi_2O_6{\cdot}H_2O\ (Anl) \quad (3)$$

We have studied the secondary alterations of nepheline and sodalite in the main rock types of the Lovozero massif. Petrographic evidence indicates that an association of zeolites (natrolite ± paranatrolite) and Al-O-H phases (nordstrandite and böhmite) was

formed as a result of the alteration of nepheline and sodalite. Indeed, according to Putnis [27], the evidence for interfaces-coupled dissolution–precipitation reactions is as follows:

- The dissolution and precipitation are closely spatially coupled at the interface between the parent and the product phases. This coupling preserves the external morphology of the parent». In this study, the preservation of the external morphology of nepheline can be seen in Figures 5f and 6a.
- The reaction front between parent and product is sharp, with no significant diffusion profile in the parent». In our study, the boundaries between parents (nepheline or sodalite) and products (zeolites and Al-O-H phases) are sharp (for example, Figures 3d, 5c,f, and 9a–c).
- The product phase develops intracrystalline porosity and permeability, which allows the fluid to maintain contact with the reaction front». In this study, the porosity of the zeolites + Al-O-H phases aggregates is clearly visible; for example, in Figures 6f and 3d.
- In cases where there is a large increase or decrease in the solid molar volume, reaction-induced fracturing produces a network of fractures ahead of the reaction front». The network of fractures ahead of the reaction front is shown, for example, in Figures 3c and 9a,b.
- In cases where the product phase has a different crystal structure to the parent, the product may be polycrystalline». In all of the studied samples, secondary natrolite and paranatrolite are represented by a fine-grained aggregate.

The replacement reactions (Figure 9) of nepheline and sodalite can be written as follows:

$$3NaAlSiO_4 + 4H_2O \Rightarrow Na_2Al_2Si_3O_{10}\cdot 2H_2O + Al(OH)_3 + NaOH \quad (4)$$

$$6NaAlSiO_4 + 9H_2O \Rightarrow Na_2Al_2Si_3O_{10}\cdot 2H_2O + Na_2Al_2Si_3O_{10}\cdot 3H_2O + 2Al(OH)_3 + 2NaOH \quad (5)$$

$$Na_4(Si_3Al_3)O_{12}Cl + 4H_2O \Rightarrow Na_2Al_2Si_3O_{10}\cdot 2H_2O + Al(OH)_3 + NaOH + NaCl \quad (6)$$

The main differences between Reactions (4)–(6) and Reactions (1) and (2) are as follows. Firstly, in addition to zeolites, the products of the reaction are Al-rich phases, such as nordstrandite and böhmite, and secondly, a third of nepheline's sodium (or sodalite's sodium) is set free and passes into fluid. In Reactions (4)–(6), we wrote this released sodium in the form of NaOH.

The results of the measurements of the areas occupied by natrolite and nordstrandite (Figure 7) confirmed the correctness of the proposed reactions. Indeed, in accordance with the reaction $3NaAlSiO_4 + 4H_2O \Rightarrow Na_2Al_2Si_3O_{10}\cdot 2H_2O + Al(OH)_3 + NaOH$ (Figure 9a), upon the substitution of 100 cm^3 of nepheline, 105 cm^3 of natrolite and 20 cm^3 of nordstrandite were formed (the volume increase is 25%; for the details of the calculation, see Table S1 in Supplementary Materials). Thus, the ratio of the volumes of natrolite and nordstrandite is 105/20 = 5.25. According to our measurements in natural samples, the median ratio of natrolite and nordstrandite volumes is 0.84/0.16 = 5.25.

Changes in volume occur in all the reactions shown in Figure 9. In reaction $6NaAlSiO_4 + 9H_2O \Rightarrow Na_2Al_2Si_3O_{10}\cdot 2H_2O + Na_2Al_2Si_3O_{10}\cdot 3H_2O + 2Al(OH)_3 + 2NaOH$ (Figure 9b), the breakdown of 100 cm^3 of nepheline produces 52 cm^3 of natrolite, 56 cm^3 of paranatrolite, and 20 cm^3 of nordstrandite, i.e., the volume increase is 30%. In reaction $Na_4(Si_3Al_3)O_{12}Cl + 4H_2O \Rightarrow Na_2Al_2Si_3O_{10}\cdot 2H_2O + Al(OH)_3 + NaOH + NaCl$ (Figure 9c), the substitution of 100 cm^3 of sodalite yields 80 cm^3 of natrolite and 15 cm^3 of nordstrandite (the volume decrease is 5%). Changes in the volume upon the alteration of feldspathoids are confirmed by microtextural observations. The fine-grained mass of zeolites and Al-O-H phases contains numerous microcracks (Figures 3d, 5f, 6f, and 9a,c). According to field observations, rocks containing intensely altered nepheline and sodalite are loose and easily destroyed.

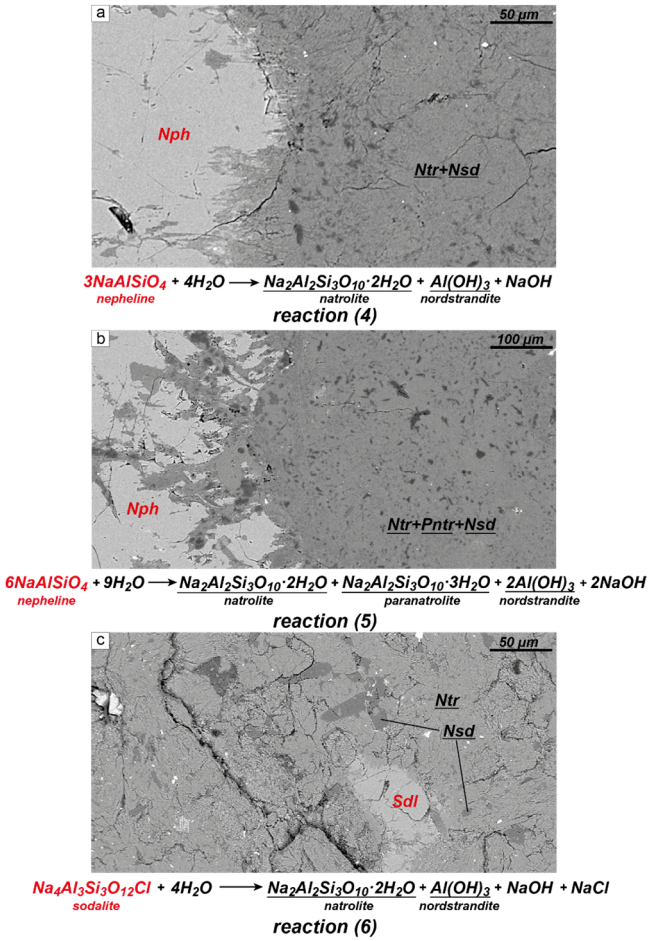

Figure 9. Proposed substitution reactions for nepheline and sodalite via an association of secondary minerals. (**a**) Replacement of nepheline with natrolite and nordstrandite (sample LV-319A, see also Figure 3); (**b**) replacement of nepheline with natrolite, paranatrolite, and nordstrandite (sample LV-319G, see also Figure 5 a,b); (**c**) replacement of sodalite with natrolite and nordstrandite (sample LV-356/3, see also Figure 6 e,f). BSE images.

Speciation calculations [9] show that the pH in the fluids of the system Na–Al–Si–O–H–Cl mainly depends on the Na/Cl ratio and, to a lesser degree, on salinity and temperature. If the Na/Cl ratio is greater than 1, the pH (at 400 °C) lies between 7 and 12. The Na/Cl ratio may change as a result of the dissolution of Cl-free or Cl-poor sodium silicates. Markl and Baumgartner [9] studied the substitution of nepheline by analcime in the rocks of the Ilimaussaq complex and concluded that the replacement is rather volume- than mass-conserving and hence that the replacement Reaction (3) should be re-formulated as follows:

$$1.85\text{Nph} + 2.3\text{H}_2\text{O} + 0.19\text{H}_4\text{SiO}_4 \Rightarrow 1.02\text{Anl} + 0.83\text{Na}^+ + 0.83\text{Al(OH)}^-_4 \quad (7)$$

As a result of Reaction (3), the pH of the fluid does not change, while in Reaction (7), slightly less than half of the sodium from the nepheline is set free and passes into the aqueous fluid. This process leads to an increase in the Na/Cl ratio and, hence, the pH of the fluid. At extremely high pH values, minerals of the so-called 'hyperagpaitic' association crystallize, such as ussingite, tugtupite, naujakasite, villiaumite, natrosilite, thermonatrite, trona, and others [28,29]. Hyperagpaitic minerals, of course, are not direct products of alteration of aluminosilicates, in particular, nepheline. However, the nepheline alteration causes a significant change in the fluid composition (pH increases), which in turn, leads to the stabilization and crystallization of hyperagpaitic minerals.

The proposed Reactions (4)–(6) are generally similar to Reaction (7). The main difference is that in Reaction (7), aluminum is present as $Al(OH)^-_4$ species, while we observe

nordstrandite $Al(OH)_3$. It is important to note that the replacement of feldspathoids by the natrolite + Al-O-H phases association is apparently not a unique feature of the Lovozero massif. Studies of the secondary alteration of sodalite in the foid syenites of the Mont Saint-Hilaire massif [11] showed that sodalite is rimmed and replaced by natrolite, which is intergrown with an Al-rich phase (page 2153, Figure 3b in [11]). It can be assumed that such an association of secondary minerals was formed through Reaction (6).

Thus, in Reaction (4), due to the release of sodium, the pH of the fluid increases. In addition, in Reaction (4), the anhydrous nepheline is replaced by natrolite-containing water molecules. As a result, the salinity of the fluid increases. The replacement of nepheline with the association between natrolite + paranatrolite + nordstrandite leads to an even greater increase in salinity since paranatrolite contains three water molecules. The intensive crystallization of zeolites can lead to fluid "drying" and the precipitation of water-soluble minerals such as villiaumite (NaF). The alteration of sodalite {reaction (6)} seems to result in a less dramatic change in pH since there is no significant increase in the Na/Cl ratio.

We assume that the secondary alteration of nepheline and sodalite in the rocks of the Lovozero massif leads to an increase in the pH of the late-magmatic fluid. As a result, the minerals of the hyperagpaitic association, such as ussingite, villiaumite, natrosilite, thermonatrite, trona, and others, can precipitate from such a fluid. Once again, we note that hyperagpaitic minerals are not direct products of nepheline or sodalite alteration. However, the secondary alteration of feldspathoids is one of the possible reasons for the occurrence of hyperagpaitic mineral associations.

The fluid can remain in the rock, and then the hyperagpaitic minerals crystallize in the immediate vicinity of the destroyed nepheline. It is for this reason that sodium loss is not observed when comparing the compositions of fresh and altered urtite using the isocon method (Figure 8a). It is also likely that fluid can move along grain boundaries or microcracks. As an example, Figure 10 shows the proposed scheme for the formation of a thermonatrite crust on the surface of a foyaite sample. We assume that the decomposition of nepheline occurs in accordance with the Reaction (4). Sodium is set free and passes into a fluid that can migrate along grain boundaries or microcracks. Thermonatrite is crystallized by the reaction of sodium (NaOH) and carbon dioxide from the atmospheric air.

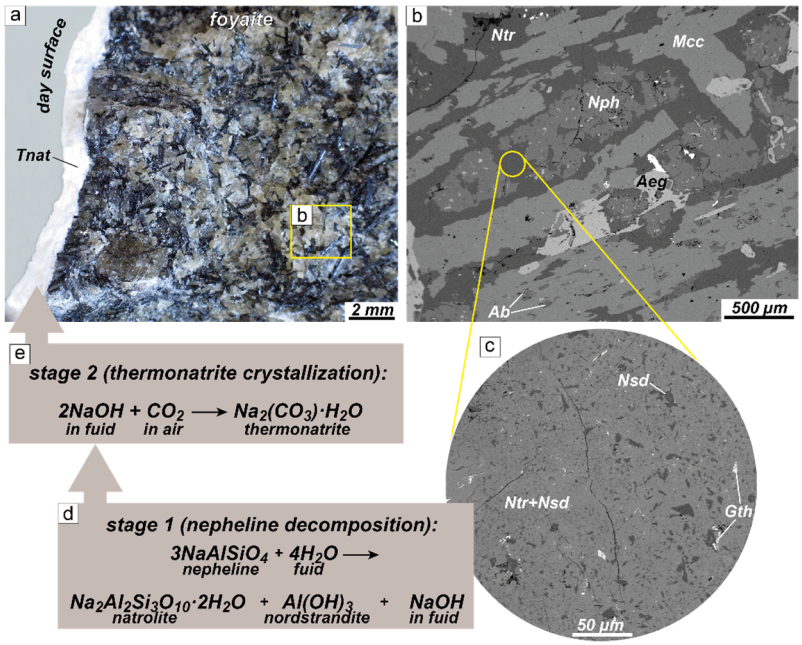

Figure 10. Scheme of the formation of a thermonatrite crust on the surface of a foyaite sample (LV-420, sample point 1 on Figure 1). (**a**) Photo of a sample of foyaite, on the surface of which there is a

crust of thermonatrite (diagnosed based on X-ray data) up to 2 mm thick; (**b**) BSE image of a fragment of a foyaite sample; nepheline is substituted by the association between natrolite + nordstrandite; (**c**) BSE image of a detailed fragment of Figure 10b; (**d**) reaction of replacement of nepheline by the natrolite + nordstrandite association (stage 1); (**e**) thermonatrite formation reaction (stage 2).

6. Conclusions

1. During the late-stage (auto)metasomatic alterations of peralkaline rocks, nepheline and sodalite are replaced by the association between natrolite + nordstrandite ± paranatrolite ± böhmite. This process occurs in all main rock types of the Lovozero massif.
2. The substitutions of nepheline and sodalite occur according to the following reactions: $3Nph + 4H_2O \rightarrow Ntr + Nsd + NaOH$; $6Nph + 9H_2O \rightarrow Ntr + Pntr + 2Nsd + 2NaOH$; $Sdl + 4H_2O \rightarrow Ntr + Nsd + NaOH + NaCl$.
3. In these reactions, about one-third of the sodium from nepheline (and sodalite) is set free and passes into the fluid. This leads to an increase in the Na/Cl ratio and, hence, the pH of the fluid.
4. An increase in pH stabilizes hyperagpaitic minerals, which can crystallize in close proximity to pseudomorphized nepheline and sodalite.

Supplementary Materials: The following supporting information can be downloaded at: https://www.mdpi.com/article/10.3390/min13010039/s1. Table S1: Calculations of volume changes during alteration reactions.

Author Contributions: Conceptualization, J.A.M. and L.M.L.; investigation, Y.A.P., L.M.L., and E.A.S.; resources, J.A.M.; data curation, J.A.M. and L.M.L.; writing—original draft preparation, J.A.M.; writing—review and editing, Y.A.P., L.M.L., and E.A.S.; visualization, Y.A.P. and L.M.L. All authors have read and agreed to the published version of the manuscript.

Funding: This research was funded by the Russian Science Foundation, project no. 21-47-09010.

Data Availability Statement: Not applicable.

Acknowledgments: We are grateful to reviewers from MDPI who helped us to improve the presentation of our results.

Conflicts of Interest: The authors declare no conflicts of interest.

References

1. LeMaitre, R.W. *Igneous Rocks. A Classification and Glossary of Terms. Recommendations of the International Union of Geological Sciences Subcommission on the Systematics of Igneous Rocks*; LeMaitre, R.W., Ed.; Cambridge University Press: Cambridge, MA, USA, 2005.
2. Marks, M.A.; Markl, G. A Global Review on Agpaitic Rocks. *Earth Sci. Rev.* **2017**, *173*, 229–258. https://doi.org/10.1016/j.earscirev.2017.06.002.
3. Kramm, U.; Kogarko, L.N. Nd and Sr Isotope Signatures of the Khibina and Lovozero Agpaitic Centres, Kola Alkaline Province, Russia. *Lithos* **1994**, *32*, 225–242. https://doi.org/10.1016/0024-4937(94)90041-8.
4. Marks, M.; Vennemann, T.; Siebel, W.; Markl, G. Nd-, O-, and H-Isotopic Evidence for Complex, Closed-System Fluid Evolution of the Peralkaline Ilímaussaq Intrusion, South Greenland. *Geochim. Cosmochim. Acta* **2004**, *68*, 3379–3395. https://doi.org/10.1016/j.gca.2003.12.008.
5. Nielsen, T.F.D. Alkaline Dyke Swarms of the Gardiner Complex and the Origin of Ultramafic Alkaline Complexes. *Geochem. Int.* **1994**, *31*, 37–56.
6. Kogarko, L.N. Ore-Forming Potential of Alkaline Magmas. *Lithos* **1990**, *26*, 167–175. https://doi.org/10.1016/0024-4937(90)90046-4.
7. Sørrensen, H. Agpaitic Nepheline Syenites: A Potential Source of Rare Elements. *Appl. Geochem.* **1992**, *7*, 417–427. https://doi.org/10.1016/0883-2927(92)90003-L.
8. Sorensen, H. The Agpaitic Rocks—An Overview. *Miner. Mag* **1997**, *61*, 485–498.
9. Markl, G.; Baumgartner, L. PH Changes in Peralkaline Late-Magmatic Fluids. *Contrib. Mineral. Petrol.* **2002**, *144*, 331–346. https://doi.org/10.1007/s00410-002-0401-6.
10. Weisenberger, T.; Spürgin, S.; Lahaye, Y. Hydrothermal Alteration and Zeolitization of the Fohberg Phonolite, Kaiserstuhl Volcanic Complex, Germany. *Int. J. Earth Sci.* **2014**, *103*, 2273–2300. https://doi.org/10.1007/s00531-014-1046-1.

11. Schilling, J.; Marks, M.A.W.; Wenzel, T.; Vennemann, T.; Horváth, L.; Tarassoff, P.; Jacob, D.E.; Markl, G. The Magmatic to Hydrothermal Evolution of the Intrusive Mont Saint-Hilaire Complex: Insights into the Late-Stage Evolution of Peralkaline Rocks. *J. Petrol.* **2011**, *52*, 2147–2185. https://doi.org/10.1093/petrology/egr042.
12. Mitchell, R.H.; Wu, F.Y.; Yang, Y.H. In Situ U-Pb, Sr and Nd Isotopic Analysis of Loparite by LA-(MC)-ICP-MS. *Chem. Geol.* **2011**, *280*, 191–199. https://doi.org/10.1016/j.chemgeo.2010.11.008.
13. Wu, F.Y.; Yang, Y.H.; Marks, M.A.W.; Liu, Z.C.; Zhou, Q.; Ge, W.C.; Yang, J.S.; Zhao, Z.F.; Mitchell, R.H.; Markl, G. In Situ U-Pb, Sr, Nd and Hf Isotopic Analysis of Eudialyte by LA-(MC)-ICP-MS. *Chem. Geol.* **2010**, *273*, 8–34. https://doi.org/10.1016/j.chemgeo.2010.02.007.
14. Korchak, Y.A.; Men'shikov, Y.P.; Pakhomovskii, Y.A.; Yakovenchuk, V.N.; Ivanyuk, G.Y. Trap Formation of the Kola Peninsula. *Petrology* **2011**, *19*, 87–101. https://doi.org/10.1134/S0869591111010036.
15. Gerasimovsky, V.I.; Volkov, V.P.; Kogarko, L.N.; Polyakov, A.I.; Saprykina, T.V.; Balashov, Y.A. *Geochemistry of the Lovozero Alkaline Massif*; Nauka: Moscow, Russia, 1966.
16. Bussen, I.V.; Sakharov, A.S. *Petrology of the Lovozero Alkaline Massif*; Nauka: Leningrad, Russia, 1972.
17. Vlasov, K.A.; Kuzmenko, M.V.; Eskova, E.M. *Lovozero Alkaline Massif*; Academy of Sciences SSSR: Moskow, Russia, 1959.
18. Lafuente, B.; Downs, R.T.; Yang, H.; Stone, N. The Power of Databases: The RRUFF Project. In *Highlights in Mineralogical Crystallography*; Armbruster, T., Danisi, R.M., Eds.; W. De Gruyter: Berlin, Germany, 2015; pp. 1–30.
19. Warr, L.N. IMA-CNMNC Approved Mineral Symbols. *Miner. Mag.* **2021**, *85*, 291–320. https://doi.org/10.1180/mgm.2021.43.
20. Johnsen, O.; Grice, J.D. The Crystal Chemistry of the Eudialyte Group. *Can. Mineral.* **1999**, *37*, 865–891.
21. Pekov, I.V.; Turchkova, A.G.; Lovskaya, E.V.; Chukanov, N.V. *Zeolites of Alkaline Massifs*; Association "Ekost'': Moskow, Russia, 2004.
22. Chao, G.Y. Paranatrolite, a New Zeolite from Mount St-Hilaire, Quebec. *Can Miner.* **1980**, *18*, 85–88.
23. Seryotkin, Y.V.; Bakakin, V.V.; Belitsky, I.A. The Crystal Structure of Paranatrolite. *Eur. J. Mineral.* **2004**, *16*, 545–550. https://doi.org/10.1127/0935-1221/2004/0016-0545.
24. Grant, J.A. The Isocon Diagram-a Simple Solution to Gresens' Equation for Metasomatic Alteration. *Econ. Geol.* **1986**, *81*, 1976–1982. https://doi.org/10.2113/GSECONGEO.81.8.1976.
25. Grant, J.A. Isocon Analysis: A Brief Review of the Method and Applications. *Phys. Chem. Earth* **2005**, *30*, 997–1004. https://doi.org/10.1016/j.pce.2004.11.003.
26. Fall, A.; Bodnar, R.J.; Szabó, C.; Pál-Molnár, E. Fluid Evolution in the Nepheline Syenites of the Ditrău Alkaline Massif, Transylvania, Romania. *Lithos* **2007**, *95*, 331–345. https://doi.org/10.1016/j.lithos.2006.08.005.
27. Putnis, A. Mineral Replacement Reactions. *Rev. Miner. Geochem* **2009**, *70*, 87–124. https://doi.org/10.2138/rmg.2009.70.3.
28. Khomyakov, A.P. *Mineralogy of Hyperagpaitic Alkaline Rocks*; Oxford University Press: Oxford, UK, 1995.
29. Khomyakov, A.P. Salt Minerals in Ultra-Agpaitic Rocks and Ore Potential of Alkaline Massifs. *Int. Geol. Rev.* **1987**, *29*, 1446–1456. https://doi.org/10.1080/00206818709466238.